The FEBS Journal

FEBS PRESS science publishing by scientists

The endoglycosidase activity of Dispersin B is mediated through electrostatic interactions with cationic poly-β-(1→6)-*N*-acetylglucosamine

Alexandra P. Breslawec, Shaochi Wang*, Kathleen N. Monahan, Lucas L. Barry and Myles B. Poulin

Department of Chemistry and Biochemistry, University of Maryland at College Park, MD, USA

Keywords
biofilm dispersal; Dispersin B; exopolysaccharides; glycoside hydrolase; PNAG

Correspondence
M. B. Poulin, Department of Chemistry and Biochemistry, University of Maryland, College Park, Maryland 20742, USA
Tel: +1 (301) 405-1811
E-mail: mpoulin@umd.edu

***Present address**
Clinical Systems Biology Laboratories, The First Affiliated Hospital of Zhengzhou University, China

(Received 7 April 2022, revised 28 July 2022, accepted 8 September 2022)

doi:10.1111/febs.16624

Bacterial biofilms consist of bacterial cells embedded within a self-produced extracellular polymeric substance (EPS) composed of exopolysaccharides, extra cellular DNA, proteins and lipids. The enzyme Dispersin B (DspB) is a CAZy type 20 β-hexosaminidase enzyme that catalyses the hydrolysis of poly-*N*-acetylglucosamine (PNAG), a major biofilm polysaccharide produced by a wide variety of biofilm-forming bacteria. Native PNAG is partially de-*N*-acetylated, and the degree of deacetylation varies between species and dependent on the environment. We have previously shown that DspB is able to perform both endo- and exo-glycosidic bond cleavage of PNAG depending on the de-*N*-acetylation patterns present in the PNAG substrate. Here, we used a combination of synthetic PNAG substrate analogues, site-directed mutagenesis and *in vitro* biofilm dispersal assay to investigate the molecular basis for the endo-glycosidic cleavage activity of DspB and the importance of this activity for dispersal of PNAG-dependent *Staphylococcus epidermidis* biofilms. We found that D242 contributes to the endoglycosidase activity of DspB through electrostatic interactions with cationic substrates in the −2 binding site. A $DspB_{D242N}$ mutant was highly deficient in endoglycosidase activity while maintaining exoglycosidase activity. When used to disperse *S. epidermidis* biofilms, this $DspB_{D242N}$ mutant resulted in an increase in residual biofilm biomass after treatment when compared to wild-type DspB. These results suggest that the de-*N*-acetylation of PNAG in *S. epidermidis* biofilms is not uniformly distributed and that the endoglycosidase activity of DspB is required for efficient biofilm dispersal.

Introduction

Bacterial biofilms consist of bacterial cells embedded in a self-assembled matrix of lipids, proteins, DNA and exopolysaccharides, known as the extracellular polymeric substance (EPS) [1]. Biofilms are beneficial to the survival of bacteria in a variety of environments, as they facilitate cell–cell adhesion and act as a protective barrier [2–5]. The biofilm EPS shields bacteria from the host immune response and contributes to antibiotic resistance [6–8]. The protection afforded by the biofilm EPS makes bacterial

Abbreviations
CAZy, Carbohydrate Active enZYmes; DspB, Dispersin B; EPS, extracellular polymeric substance; ESI-MS, electrospray ionization mass spectrometry; GH, glycosyl hydrolase; Glc, glucose; GlcN, glucosamine; GlcNAc, *N*-acetylglucosamine; MALDI-TOF, matrix assisted laser desorption ionization time of flight; NMR, nuclear magnetic resonance; PIA, polysaccharide intracellular adhesin; PNAG, poly-β-(1→6)-*N*-acetylglucosamine; TLC, thin-layer chromatography; TSB, tryptic soy broth.

biofilm infections difficult to treat, and as a result, biofilms contribute to an estimated 65% of all microbial infections in humans and up to 80% of chronic infections [9–11]. Thus, there is a need for therapeutics that specifically target bacterial biofilms by either preventing biofilm formation or disrupting existing biofilms [12–15].

Compounds that disperse biofilms are known as dispersal agents, and many, including the enzyme Dispersin B (DspB) [16] are being explored for their potential anti-biofilm properties. DspB is a native β-hexosaminidase enzyme of *Aggregatibacter actinomycetemcomitans* that hydrolyses the exopolysaccharide poly-β-(1→6)-*N*-acetylglucosamine (PNAG, also known as polysaccharide intracellular adhesin, PIA) [16–18]. PNAG is a common structural component of the biofilm EPS produced by both Gram-positive and Gram-negative human pathogens including *Staphylococcus epidermidis* [19,20], *Staphylococcus aureus* [21], *Escherichia coli* [22], *Klebsiella pneumoniae* [23] and *Acinetobacter baumannii* [24]. Native PNAG is partially de-*N*-acetylated and periodically *O*-succinylated during its biosynthesis through the action of carbohydrate esterase enzymes and yet unidentified succinyltransferase enzymes, respectively, though the relative abundance and patterning of these modifications will vary depending on the bacterial species and growth conditions [20,25–27]. PNAG is essential to both the structure of the biofilms in which they are found, as well as the overall virulence of the bacteria [7,17,20,22,28,29]. Thus, enzymes capable of hydrolysing PNAG, such as DspB and the glycosyl hydrolase (GH) domain of PgaB, are very interesting enzymes to investigate for their possible use as anti-biofilm treatments [16,30]. However, this requires a detailed understanding of the substrate specificity of these enzymes.

We previously found that both the mechanism and product distribution for DspB-catalysed hydrolysis of PNAG is dependent on the de-*N*-acetylation patterns present within the PNAG substrate [31]. Specifically, fully *N*-acetylated PNAG oligosaccharides (i.e. **1**) are hydrolysed predominantly through sequential exo-glycosidic bond cleavage at the non-reducing end GlcNAc [31], which is enhanced by approximately three-fold as a result of electrostatic interactions between DspB and substrates containing a cationic glucosamine (GlcN) in the +2 position relative to the site of cleavage [32]. Moreover, we found that in the presence of non-reducing terminal GlcN (i.e. **2**) residues, DspB performs endo-glycosidic bond cleavage at the next available GlcNAc residue at a rate that is nearly identical to the rate of exo-glycosidic bond cleavage of fully acetylated trisaccharide **1**. The ability of DspB to perform endo-glycosidic bond cleavage of PNAG is likely critical for its biofilm dispersal activity given that native PNAG is partially de-*N*-acetylated [7], yet the mechanism of substrate recognition for this endoglycosidase activity of DspB remains unclear. Herein, we use detailed kinetic measurements with synthetic PNAG trisaccharide analogues combined with site-directed mutagenesis and *in vitro* biofilm dispersal assays to explore the molecular basis for the endoglycosidase activity of DspB and assess the importance of this activity for the DspB-catalysed dispersal of *S. epidermidis* biofilms.

Results and Discussion

In previous studies, we measured the observed rate constant (k_1) for DspB-catalysed hydrolysis of **1** by fitting the disappearance of trisaccharide to a single exponential (Eqn 1) under conditions where the concentration of trisaccharide is well below K_M [31,32]:

$$[T] = [T_0] \times e^{(-k_1[E_0]t)} \quad (1)$$

where $[T]$ is the concentration of trisaccharide substrate at time t, $[T_0]$ is the initial trisaccharide concentration and $[E_0]$ is the initial enzyme concentration. Under these conditions, k_1 is proportional to the enzyme specificity constant k_{cat}/K_M and represents a pseudo-second-order rate constant for hydrolysis of the trisaccharide [31]. However, this analysis assumes that the rate of trisaccharide consumption occurs exclusively via a single exo-glycosidic bond cleavage mechanism, or that the rate of endo-glycosidic bond cleavage does not contribute significantly to the observed rate constant. Previous studies of DspB kinetics on fully acetylated PNAG disaccharide–pentasaccharide analogues suggest that endo-glycosidic bond cleavage can occur on trisaccharide or larger substrates [33].

To evaluate the contributions of exo- and endglycosidic bond cleavage of **1** greater detail, we numerically fit the change in reducing end trisaccharide, disaccharide and monosaccharide product concentrations observed during the hydrolysis of **1** by DspB (Fig. 1A) to a series of differential equations describing either a two-parameter model that assumes that cleavage occurs exclusively via sequential exo-glycosidic bond cleavage (Eqn 2), or to a three-parameter that includes endo-glycosidic cleavage (Eqn 3):

$$\frac{d[T]}{dt} = -k_1[E_0][T]; \frac{d[D]}{dt} = k_1[E_0][T] - k_2[E_0][D]; \frac{d[M]}{dt} = k_2[E_0][D] \quad (2)$$

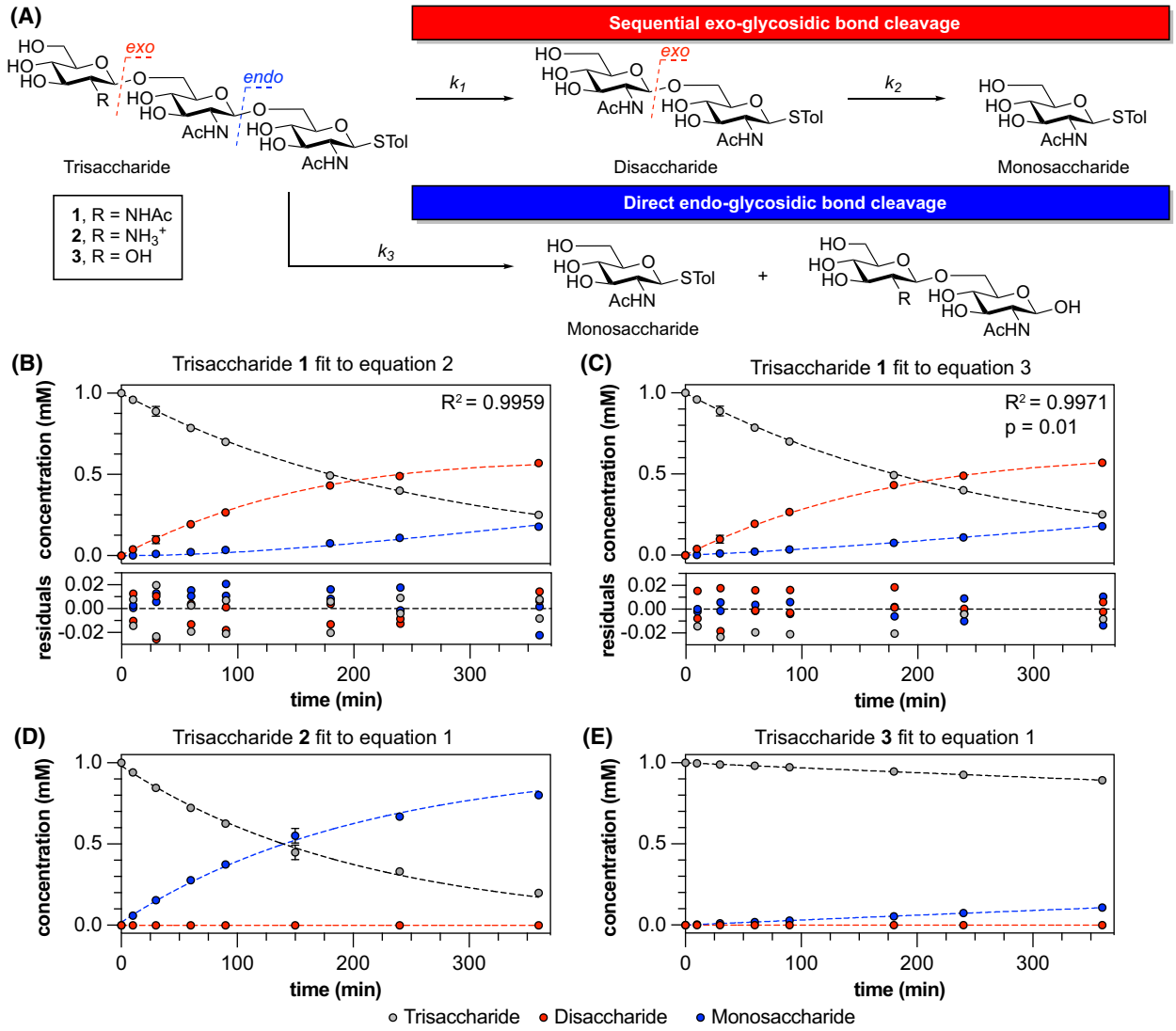

Fig. 1. Mechanisms of DspB catalysed hydrolysis of PNAG. (A) model for DspB catalysed hydrolysis of PNAG analogues **1**–**3** highlighting the rates of sequential exo-glycosidic bond cleavage (k_1 and k_2) or endo-glycosidic bond cleavage (k_3). (B, C) Reaction progress curves for the hydrolysis of **1** by $DspB_{wt}$ fit using Eqn (2) (B) or Eqn (3) (C). A statistically significant improvement in the fit to Eqn (3). Errors represent the standard deviation from two replicate measurements and residuals are shown. (D) Reaction progress curves for the hydrolysis of **2** by $DspB_{wt}$ fit using Eqn (1). (E) Reaction progress curves for the hydrolysis of **3** by $DspB_{wt}$ fit using Eqn (1). Individual rate constants are summarized in Table 1.

$$\begin{aligned}\frac{d[T]}{dt} &= -k_1[E_0][T] - k_3[E_0][T];\\ \frac{d[D]}{dt} &= k_1[E_0][T] - k_2[E_0][D];\\ \frac{d[M]}{dt} &= k_3[E_0][T] + k_2[E_0][D]\end{aligned} \tag{3}$$

where $[T]$, $[D]$ and $[M]$ are the concentrations of the reducing end trisaccharide, disaccharide and monosaccharide, respectively. When $[T_0] \geq K_M$, which is the case in our experiments, the observed rate constants (k_1, k_2 and k_3) are proportional to k_{cat}/K_M for the exo-glycosidic bond cleavage of the trisaccharide substrate, exo-glycosidic bond cleavage of disaccharide intermediate and endo-glycosidic bond cleavage of the trisaccharide substrate, respectively. An analogous numerical fitting approach was used to approximate the rate constants for cleavage of fully acetylated PNAG analogues [33], and allows us to evaluate the contribution of both exo- and endo-glycosidic bond cleavage to the observed rate of disappearance of trisaccharide **1** catalysed by DspB.

Numerical fitting to the three-parameter model (Fig. 1C, Table 1) showed a statistically significant improvement compared to the fit to the two-parameter model (Fig. 1B, Table 1). The rate of endo-glycosidic cleavage of **1** (0.31 $M^{-1}{\cdot}s^{-1}$) is nearly 13 times slower than the rate of exo-glycosidic cleavage (3.95 $M^{-1}{\cdot}s^{-1}$), and more than 3 times slower than exo-glycosidic cleavage of the reducing end disaccharide intermediate (1.03 $M^{-1}{\cdot}s^{-1}$). These results support our previous observation that trisaccharide cleavage occurs predominantly through exo-glycosidic bond cleavage [31,32]. For the hydrolysis of **2**, which lacks an acetamido group on the non-reducing sugar, only endo-glycosidic cleavage is observed (Fig. 1D, Table 1) at a rate 18 times faster than observed for the endo-glycosidic cleavage of **1**. This suggests that DspB may possess a discrete −2 binding site with specificity for binding GlcN.

To evaluate this hypothesis, we synthesized PNAG trisaccharide analogue **3** containing a non-reducing terminal glucose (Glc). Trisaccharide **3** does not contain the necessary acetamido group on the non-reducing residue that is required for the substrate assisted cleavage mechanism but lacks the cationic amine of GlcN. Trisaccharide **3** was synthesized using the same iterative one-pot glycosylation strategy used for the synthesis of trisaccharides **1** and **2** and isolated in 50% overall yield from the corresponding monosaccharide building blocks **4** and **5** after deprotection (Scheme 1).

As with **2**, we observed only endo-glycosidic bond cleavage of **3** by DspB (Fig. 1E) at a rate that is nearly identical to the rate of endo-glycosidic bond cleavage observed for hydrolysis of **1** (Table 1). Thus, the enhanced rate of endo-glycosidic bond cleavage observed for hydrolysis of **2** likely results from electrostatic interactions between anionic amino acids in the −2 binding site of DspB and the amino group of **2**, which would be cationic at the optimum pH of DspB (pH 6.0). There are three anionic amino acids, D242, E332 and D333, that are predicted to be within ~ 6 Å of C6 of GlcNAc in the active site of DspB (Fig. 2A). To test for their potential role in the recognition of GlcN in the −2 binding site of DspB and enhancing the rate of endo-glycosidic bond cleavage, each residue was mutated to the corresponding glutamine or asparagine, respectively. As seen in Fig. 2B, both the $DspB_{E332Q}$ and $DspB_{D333N}$ mutations resulted in a complete loss of activity on all substrates tested. This is perhaps not surprising as E332 is conserved as an acidic amino acid in GH20 family enzymes and was previously found to be essential for DspB activity [34]. The equivalent residue in the crystal structures of *Streptomyces plicatus* hexosaminidase (E444) and *Serratia marcescens* chitobiase (E739) form direct hydrogen bonds to the C4 hydroxyl group of GlcNAc bound in the −1 site of these enzymes [35,36].

Table 1. Observed rate constants for DspB catalysed hydrolysis of trisaccharides **1**–**3**.

Substrate		k_1 (M^{-1} s^{-1})	k_2 (M^{-1} s^{-1})	k_3 (M^{-1} s^{-1})
Tri **1**	wt	3.95 ± 0.07	1.0 ± 0.1	0.31 ± 0.05
	D242N	2.26 ± 0.01	1.09 ± 0.03	0.035 ± 0.007
Tri **2**	wt	–	–	5.1 ± 0.2
	D242N	–	–	0.91 ± 0.01
Tri**3**	wt	–	–	0.35 ± 0.01
	D242N	–	–	0.0 ± 0.0

Errors represent the standard deviation from two replicate measurements.

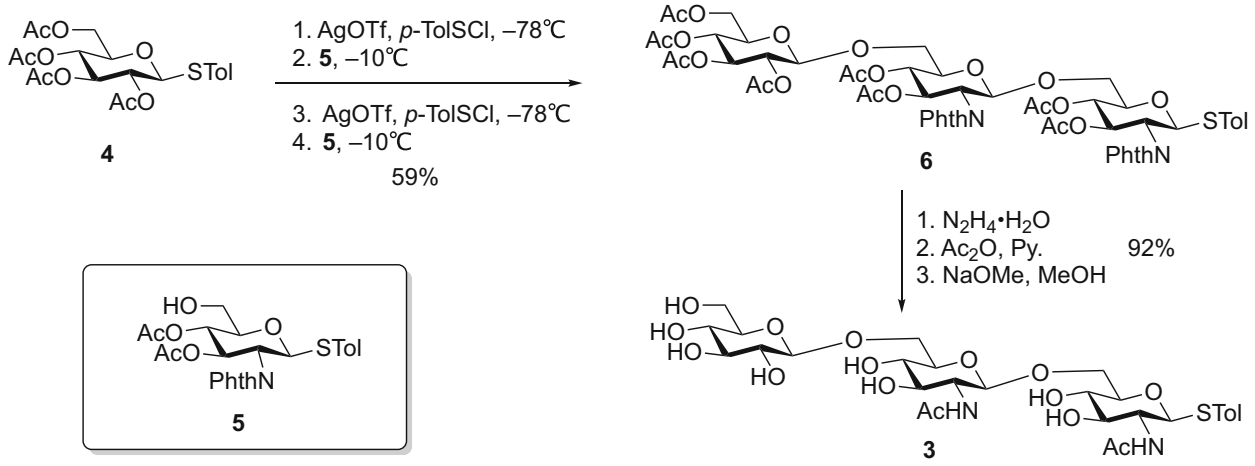

Scheme 1. Synthesis of trisaccharide **3** via iterative one-pot glycosylation.

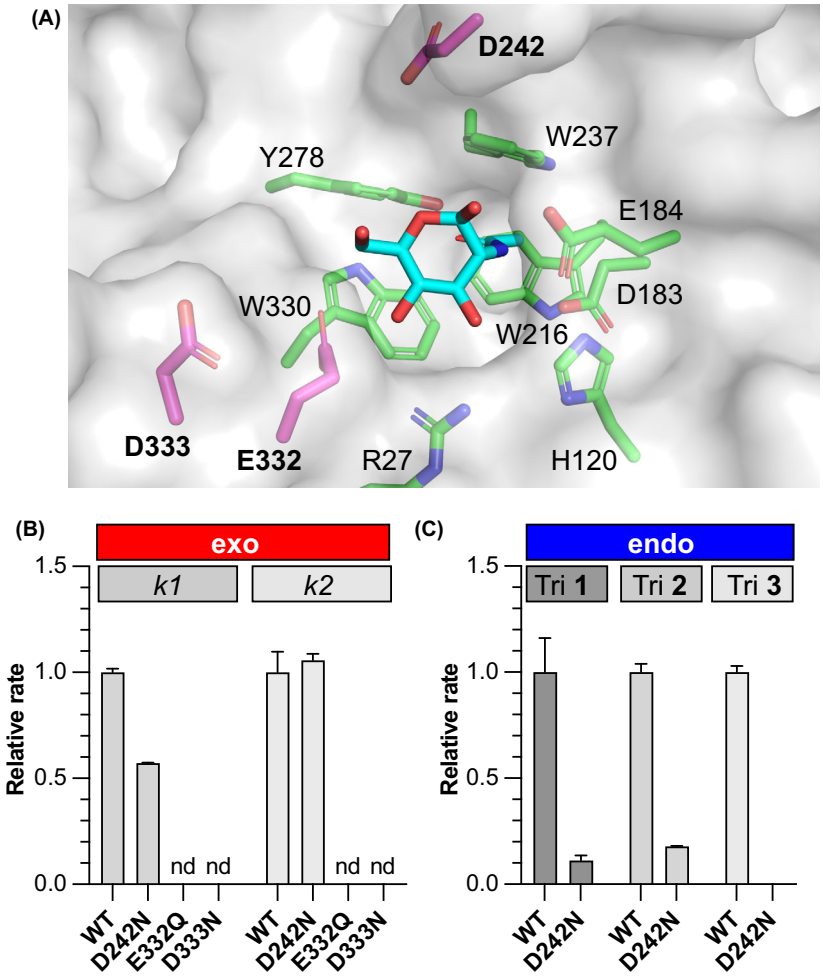

Fig. 2. Electrostatic interactions between D242 of DspB and cationic GlcN in the −2 binding site of DspB enhance endoglycosidase activity. (A) Model of DspB (1HYT) with GlcNAc modelled in the −1 binding site based on the structure of GlcNAc bound to StrH (2YL9). Key catalytic amino acid residues are shown in green. Anionic amino acids that are within 5 Å of the C6 of GlcNAc are shown in pink. The image was generated using PYMOL 2.3 (Schrödinger, New York, NY, USA). (B, C) Relative rate constants for exo- (B) and endo-glycosidic bond cleavage (C) catalysed by $DspB_{wt}$ and putative −2 site mutants. nd indicates that no hydrolysis products were detected after 6 h of incubation. Individual rate constants for each reaction are summarized in Table 1. Errors represent the standard deviation from two replicate measurements.

The D242N mutant displayed a < 50% decrease in k_1 for cleavage of trisaccharide **1** and no effect on k_2 for cleavage of the disaccharide intermediate, indicating that D242 likely has no significant role in the sequential exoglycosidase activity of DspB (Fig. 2, Table 1). Instead, we observed a significant eightfold decrease in the endo-glycosidic cleavage rate (k_3) for trisaccharide **1**, a nearly sixfold decrease in the endo-glycosidic bond hydrolysis of **2**, and no observable cleavage of **3** occurred during the 6 h the reaction was monitored. It is also important to note that reaction progress curves for hydrolysis of **1** by $DspB_{D242N}$ fit better to the two-parameter model (Eqn 2) than to the three-parameter model (Eqn 3) indicating that the effect of the D242N mutation on endoglycosidase activity of DspB may be even more substantial. These results clearly support a role for D242 in facilitating the endoglycosidase activity of DspB.

From these *in vitro* kinetic studies, we can conclude that $DspB_{D242N}$ is deficient in endoglycosidase activity with trisaccharide substrates. However, native polymeric PNAG is much larger and likely occupy an extended binding pocket on the surface of DspB when compared to trisaccharides **1**–**3**. Thus, it is probable that additional interactions also contribute to the endoglycosidase activity of DspB on polymeric PNAG. To assess the impact interaction with D242 have on the hydrolysis of native PNAG, we measured the dispersal of pre-formed *S. epidermidis* biofilms with both $DspB_{wt}$ and the $DspB_{D242N}$ mutant. Biofilms of *S. epidermidis* RP62A were grown as static cultures for 24 h in 96 well plates before being treated with increasing concentrations of either $DspB_{wt}$ or $DspB_{D242N}$ for 90 min. The residual biofilm biomass remaining after dispersal was quantified using a crystal violet dye-binding assay as described previously [32]. As seen in Fig. 3A–C, both $DspB_{wt}$ and $DspB_{D242N}$ were able to disperse biofilms of *S. epidermidis* with IC_{50} values of 14 ± 11 and 60 ± 20 pg·mL^{-1}, respectively. This suggests that the D242N mutation of DspB does not have

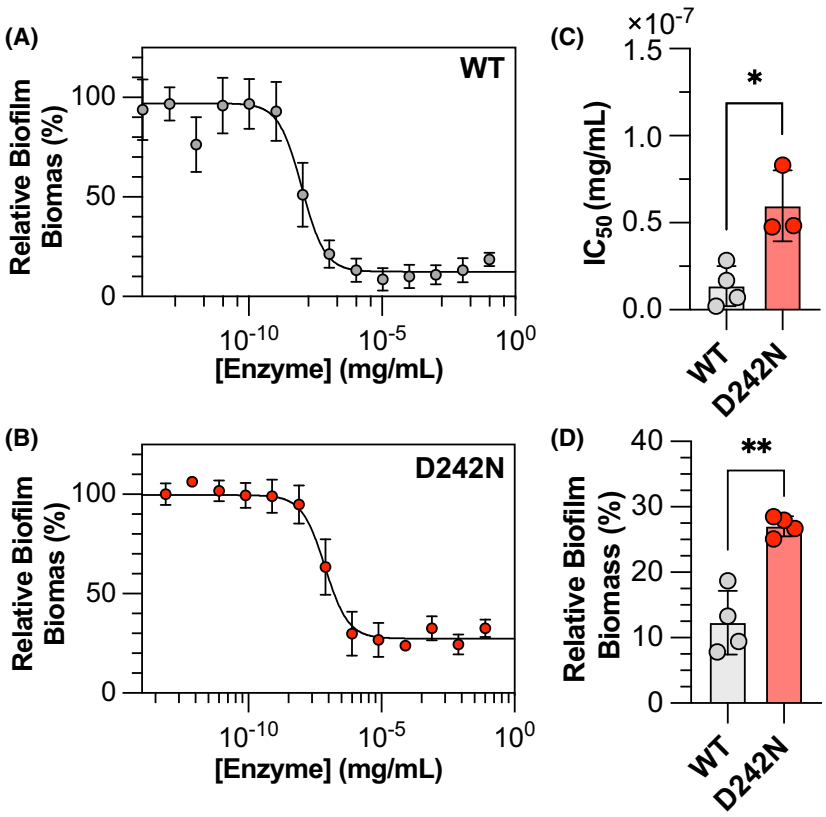

Fig. 3. Dispersal of *S. epidermidis* biofilms. IC_{50} curves for the dispersal of *S. epidermidis* RP62A biofilms with varying concentrations of $DspB_{wt}$ (A) and $DspB_{D242N}$ (B). Error bars represent the standard deviation of four biological replicates. Comparison of the biofilm IC_{50} values (C) and residual biofilm biomass remaining after dispersal with saturating concentrations of either $DspB_{wt}$ or $DspB_{D242N}$ (D). Statistical significance was determined using a Welch's *t*-test. $*P < 0.05$, $**P < 0.01$.

a large impact on the observed IC_{50} values. However, we do observe a statistically significant increase in the residual biofilm biomass remaining after dispersal with $DspB_{D242N}$ compared to $DspB_{wt}$. Even at saturating concentrations of $DspB_{wt}$ we observe $12 \pm 5\%$ biofilm biomass remaining after the dispersal of *S. epidermidis* biofilms. The residual biomass likely consists of biofilm that is not dependent on PNAG, or regions of biofilm containing PNAG resistant to DspB treatment. For biofilms treated with saturating concentrations of $DspB_{D242N,}$ we observed a statistically significant increase in the residual biofilm biomass remaining after dispersal ($27 \pm 2\%$).

A possible explanation for these observations is that the additional biofilm biomass remaining after dispersal with $DspB_{D242N}$ represents regions of biofilm containing extensively de-*N*-acetylated PNAG that is resistant to degradation. This is consistent with reports of the structure of PNAG/PIA isolated from *S. epidermidis* and *S. aureus*, which had identified different polysaccharide fractions that varied in the amount of GlcN, and *O*-succinate present in the polysaccharides [20,25,27]. In fact, in the original structural characterization of *S. epidermidis* PNAG in 1996 [20], when the isolated PNAG was fractionated on a cation exchange column it was separated into four fractions that varied between 2% and 26% GlcN, respectively, indicating that the cationic groups are not evenly distributed among PNAG polysaccharides. Our results are consistent with this uneven distribution of PNAG de-*N*-acetylation and suggests that regions of extensively de-*N*-acetylated PNAG are present in *Staphylococcal* biofilms and resistant to degradation by $DspB_{D242N}$. More work is required to confirm these findings and assess the biological significance of any non-uniform distribution of PNAG modifications.

Conclusions

DspB has been of great interest as a biofilm dispersal agent, and potential anti-biofilm therapeutic because of its ability to effectively hydrolyse PNAG and

disperse PNAG-dependent bacterial biofilms [16–18]. Here, we used enzyme kinetics measurements with synthetic PNAG trisaccharide analogues, combined with site-directed mutagenesis, and *in vitro* biofilm dispersal assays to investigate the mechanism of endo-glycosidic bond cleavage catalysed by DspB and evaluate its role in biofilm dispersal activity. Taken together, the results of these studies support a model where the rate of endo-glycosidic bond cleavage catalysed by DspB is, at least in part, regulated through electrostatic interactions between D242 and a cationic GlcN present in the −2 binding site. The $DspB_{D242N}$ mutant showed a decreased rate of endo-glycosidic bond cleavage on all synthetic PNAG analogues. Moreover, treatment of *S. epidermidis* biofilms with $DspB_{D242N}$ resulted in a greater amount of residual biofilm biomass than treatment with $DspB_{wt}$. These results support a model where PNAG modifications, including de-*N*-acetylation, are not uniformly distributed in *S. epidermidis* biofilms and instead there are regions with high de-*N*-acetylation and regions with low de-*N*-acetylation of PNAG. Future efforts to improve the biofilm dispersal activity of DspB should focus on identifying mutants with enhanced activity on highly de-*N*-acetylated PNAG. Given the altered substrate specificity of this $DspB_{D242N}$ mutant, we believe that this enzyme will also be a valuable tool to assess the biological significance of PNAG de-*N*-acetylation not only in *S. epidermidis* but in a wide variety of Gram-positive and Gram-negative human pathogens.

Materials and methods

General

All chemical reactions were carried out in oven-dried glassware under anhydrous conditions with freshly distilled solvents under a positive pressure of argon gas, and all chemicals purchased were reagent grade and used without further purification, unless otherwise noted. Chemical reactions were monitored by thin-layer chromatography (TLC). Spots were visualized by UV light (254 nm) and charring with a solution of 10% sulphuric acid in MeOH. Column chromatography was performed on silica gel (200–300 mesh). ^{1}H and ^{13}C NMR spectra were recorded at room temperature for solutions in $CDCl_3$ or D_2O on Advance III-400 or III-600 spectrometers (Bruker). ^{1}H NMR and 13C NMR chemical shifts are reported relative to residual solvent peak in parts per million (ppm). The following standard abbreviations are used to indicate multiplicity: s = singlet, d = doublet, t = triplet, m = multiplet, dd = doublet of doublets, dt = doublet of triplets, td = triplet of doublets and br = broad. ESI-MS experiments were performed on an AccuTOF-ESI mass spectrometer. MALDI-TOF mass spectra were performed on a Bruker Autoflex Speed spectrometer using trihydroxyacetophenone as the matrix, unless otherwise noted.

Synthesis of trisaccharide substrates

Trisaccharides **1** and **2**, and building blocks **4** and **5**, were prepared as described previously [31,37]. Trisaccharide **3** was synthesized in 50% overall yield from building blocks **4** and **5** as described in scheme 1.

p-Methylphenyl 2,3,4,6-tetra-*O*-acetyl-β-D-glucopyranosyl-(1→6)-3,4-di-*O*-acetyl-2-deoxy-2-phthalimido-β-D-glucopyranosyl-(1→6)-3,4-di-*O*-acetyl-2-deoxy-2-phthalimido-1-thio-β-D-glucopyranoside (6)

Compound **6** was synthesized using a modification of the iterative one-pot glycosylation method reported previously [31]. Briefly, a solution of glycosyl donor **4** (40 mg, 0.09 mmol) was dissolved in CH_2Cl_2 (2 mL) containing freshly flame-activated 4 Å molecular sieves (150 mg) and stirred at room temperature for 30 min. The reaction mixture was cooled to −78 °C and a solution of AgOTf (71 mg, 0.27 mmol) dissolved in Et_2O (1 mL) was added. After 5 min, freshly distilled *p*-TolSCl (14.5 µL, 0.11 mmol) was added using a micro-syringe. The donor was completely consumed (as judged by TLC) after 2–3 min at which point a solution of glycosyl acceptor **5** (43 mg, 0.09 mmol) in CH_2Cl_2 (0.2 mL) was added dropwise along the flask wall via a syringe. The reaction mixture was warmed to −10 °C and stirred for an additional 20 min at which point the acceptor was completely consumed. The reaction mixture was cooled back to −78 °C and AgOTf (71 mg, 0.27 mmol) dissolved in Et_2O (1 mL) was added. After 5 min, additional *p*-TolSCl (10.5 µL, 0.08 mmol) was added using a microsyringe. After the disaccharide donor was completely consumed (~ 5 min at −78 °C), a solution of acceptor **5** (0.08 mmol) in CH_2Cl_2 (0.2 mL) was added slowly and dropwise along the flask wall via a syringe. The reaction mixture was warmed to −10 °C and stirred for an additional 30 min. The final reaction mixture was diluted with CH_2Cl2 (20 mL) and the mixture was filtered through a pad of celite. The CH_2Cl_2 phase was washed successively with a saturated aqueous solution of $NaHCO_3$ (2 × 20 mL) followed by brine (2 × 10 mL). The organic layer was dried over $MgSO_4$, concentrated and purified by silica gel flash chromatography (ethyl acetate : hexanes, 2 : 3) to give 64 mg of trisaccharide **6** (59% yield) as a colourless amorphous solid. ^{1}H NMR (600 MHz, $CDCl_3$) δ 7.85–7.79 (m, 4H), 7.73 (dd, J = 5.5, 3.0 Hz, 2H), 7.65 (dd, J = 5.5, 3.0 Hz, 2H), 7.16 (d, J = 8.0 Hz, 2H), 7.08 (d, J = 8.0 Hz, 2H), 5.73 (dd, J = 10.7, 9.0 Hz, 1H), 5.64 (dd, J = 9.5,

9.4 Hz, 1H), 5.50 (d, J = 10.4 Hz, 1H, H-1), 5.48 (d, J = 8.5 Hz, 1H, H-1′), 5.29 (dd, J = 9.6, 9.5 Hz, 1H), 5.10 (dd, J = 9.7, 9.6 Hz, 1H), 5.05–5.01 (m, 2H), 4.90 (dd, J = 9.9, 9.5 Hz, 1H), 4.74 (d, J = 8.0 Hz, 1H, H-1″), 4.30 (dd, J = 10.8, 8.6 Hz, 1H), 4.27 (dd, J = 12.4, 4.8 Hz, 1H), 4.20–4.12 (m, 2H), 4.05 (dd, J = 10.7, 2.8 Hz, 1H), 3.95 (dd, J = 11.3, 2.4 Hz, 1H), 3.84 (ddd, J = 9.8, 6.6, 2.5 Hz, 2H), 3.80 (ddd, J = 10.1, 4.7, 2.3 Hz, 2H), 3.78–3.75 (m, 1H), 3.71 (dd, J = 11.3, 6.6 Hz, 1H), 3.62 (dd, J = 10.8, 5.7 Hz, 1H), 2.36 (s, 3H), 2.11 (s, 3H), 2.09 (s, 3H), 2.05 (s, 3H), 2.03 (s, 3H), 2.01 (s, 3H), 1.87 (s, 6H), 1.75 (s, 3H), 1.65 (s, 3H). ^{13}C NMR (151 MHz, CDCl3) δ 170.1, 169.6, 169.6, 169.5, 169.1, 168.9, 168.8, 168.7, 138.1, 133.7, 133.6, 133.5, 133.3, 131.0, 129.1, 126.0, 123.1, 123.0, 100.2, 97.6, 81.7, 76.2, 73.0, 72.3, 71.4, 71.0, 70.6, 70.4, 69.2, 68.7, 68.3, 67.8, 67.5, 61.3, 53.9, 53.0, 20.6, 20.2, 20.2, 20.1, 20.0, 20.0, 19.9, 19.9, 19.8. MALDI-TOF-MS for $C_{57}H_{60}N_2O_{25}SNa$ (M + Na) calcd. 1227.31, found 1227.46.

p-Methylphenyl *β*-D-glucopyranosyl-(1→6)-2-acetamido-2-deoxy-*β*-D-glucopyranosyl-(1→6)-2-acetamido-2-deoxy-1-thio-*β*-D-glucopyranoside (3)

Compound **6** (64 mg, 0.053 mmol) was treated with hydrazine monohydrate (10 mg, 0.20 mmol) in ethanol (3 mL). After stirring for 2 h at reflux, the mixture was concentrated by rotary evaporation. The resulting residue was then dissolved in pyridine (3 mL) and acetic anhydride (1.5 mL, 15.8 mmol) was added. After stirring the mixture at room temperature overnight, it was diluted to 20 mL with CH_2Cl_2, and the organic layer was washed with water, dried over $MgSO_4$ and concentrated under vacuum. The crude product was purified by silica flash chromatography (CH_2Cl_2 : MeOH = 40 : 1) to give the per-acetylated trisaccharide intermediate. This was then dissolved in a solution of 0.05 M NaOMe in MeOH (3 mL) at pH = 9. After stirring for 3 h at room temperature, the reaction mixture was neutralized by addition of Amberlite IR-120 (H+) resin. The mixture was filtered and evaporated under vacuum to give compound **3** (31 mg, 85%) as a white solid. ^{1}H NMR (400 MHz, D_2O) δ 7.33 (d, J = 8.0 Hz, 2H), 7.17 (d, J = 8.0 Hz, 2H), 4.74 (d, J = 10.5 Hz, 1H, H-1), 4.45 (d, J = 8.5 Hz, 1H, H-1′), 4.38 (d, J = 7.9 Hz, 1H, H-1″), 4.12 (d, J = 10.7 Hz, 1H), 4.09–4.02 (m, 1H), 3.89–3.85 (m, 1H), 3.83 (dd, J = 12.3, 1.8 Hz, 1H), 3.74 (dd, J = 11.7, 4.9 Hz, 1H), 3.71–3.64 (m, 3H), 3.62 (dd, J = 11.4, 4.1 Hz, 1H), 3.53–3.42 (m, 4H), 3.41–3.27 (m, 4H), 3.23 (dd, J = 9.2, 8.0 Hz, 1H), 2.25 (s, 3H), 1.95 (s, 3H), 1.89 (s, 3H). ^{13}C NMR (100 MHz, D_2O) δ _174.5, 174.2, 138.8, 132.0 (2C), 130.0 (2C), 128.5, 102.8, 101.5, 86.8, 78.8, 75.9, 75.6, 75.2, 74.8, 73.8, 73.0, 69.7, 69.6, 69.6, 68.9, 60.7, 55.4, 54.9, 54.4, 22.1, 22.1, 20.1. MALDI-TOF-MS for C29H44N2O15SNa (M + Na) calcd 715.24, found 715.25.

Protein production

Recombinant *A. actinomycetemcomitans* Dispersin B (residues 16–381, $DspB_{wt}$) was prepared as previously described [31]. The $DspB_{D242N}$ and $DspB_{E184Q}$ mutant expression plasmids were prepared by Quikchange site-directed mutagenesis (Agilent, Santa Clara, CA, USA) using the primer pairs outlined in Table 2 and confirmed by single-pass Sanger sequencing. Each mutant enzyme was prepared via recombinant expression in *E. coli* BL21(DE3) and the proteins were purified as described for $DspB_{wt}$ [31]. Protein concentrations were determined using the UV–vis absorbance at 280 nm with a calculated molar extinction coefficient of 51 340 $M^{-1}{\cdot}cm^{-1}$. All proteins were purified to > 95% purity as confirmed via SDS/PAGE, flash frozen and stored as individual aliquots at −80 °C.

Time course assays for hydrolysis of PNAG trisaccharide analogues 1–3

The hydrolysis of PNAG trisaccharide analogues **1–3** by wild-type DspB or DspB mutants was monitored by reversed phase HPLC as described previously with a few modifications [31]. Briefly, reactions containing 1 mM of trisaccharide (**1–4**) in 48 mM of potassium phosphate buffer containing 100 mM of NaCl (pH 6.0), were initiated by the addition of an appropriate concentration of $DspB_{wt}$ or DspB mutant enzyme in a final volume of 50 µL. Individual 5 µL aliquots were removed at time 0 min and after 10, 30, 60, 90, 180, 240 and 360 min incubations at 22 °C and

Table 2. Primers for site-directed mutagenesis used in this study.

Mutation		Primer sequence
D242N	fwd	5′-GCTATGACGGTGCTACCCAAGAC-3′
	rev	5′-GTCTTGGGTAGCACCGTCATAGC-3′
E332Q	fwd	5′-GCGGCGCTGAGCATTTGGGGCCAGGATGCGAAGGCGCTG-3′
	rev	5′-CAGCGCCTTCGCATCCTGGCCCCAAATGCTCAGCGCCGC-3′
E332A	fwd	5′-CAGCGCCCTTCGCATCCCGCCCCCAAATGCTCGCGCCGC-3′
	rev	5′-CAGCGCCCTTCGCATCCCGCCCCCAAATGCTCGCGCCGC-3′
D333N	fwd	5′-GCGGCGCTGAGCATTTGGGGCGAGAATGCGAAGGCGCTG-3′
	rev	5′-CAGCGCCTTCGCATTCTCGCCCCAAATGCTCAGCGCCGC-3′

quenched through the addition of 5 μL of 100 mM trifluoroacetic acid (TFA). Each 10 μL quenched fraction was then centrifuged at 17 000 ***g*** for 2 min to remove any insoluble material and diluted to 50 μL using MQ water. Each sample was analysed by reversed-phase HPLC as previously described [31]. The concentrations of trisaccharide remaining and of all reducing-end products were determined based on the relative peak areas of the absorbance at 254 nm resulting from the *S*-tolyl aglycone. Reaction rates for hydrolysis of **1** were determined by numerical fitting of the series of differential equations shown in Eqn (2) or Eqn (3) as implemented in MATLAB (MathWorks, Natick, MA, USA). An F test was used to determine whether the two-parameter or three-parameter model fit to the data best and to determine the statistical significance of the improved fit. A detailed summary of the fit statistics and residuals for $DspB_{wt}$ catalysed hydrolysis of **1** are shown in Fig. 1B,C. Reaction rates for hydrolysis of **2** and **3** that shown exclusive endo-glycosidic bond cleavage were determined using Eqn (1) to give the pseudo-second-order rate constant k_3 in units of $M^{-1}{\cdot}s^{-1}$. [32]

In vitro dispersal of *S. epidermidis* biofilms

S. epidermidis RP62A was obtained from ATCC (ATCC 35984). A starter culture was grown in 25 mL of tryptic soy broth (TSB) for 24 h at 37 °C with shaking. The culture was then diluted to an OD_{600} of 0.01 in sterile TSB and 200 μL of the diluted culture were added to each sample well of a clear, flat-bottom 96-well plate (Nunc Edge, Thermo Fisher, Waltham, MA, USA). Four wells per plate were reserved as sterile media controls and contained 200 μL of sterile TSB. MQ water was added to the outer moat to limit evaporation and edge effects during biofilm growth. Static cultures were grown by incubating the plates at 37 °C for 24 h. After 24 h, the culture media and all non-adherent cells were removed by aspiration and 200 μL of sterile 50 mM potassium phosphate buffer, pH 6.0 was added to each well. Twenty microlitres of a solution containing various dilutions of $DspB_{wt}$ or mutant enzyme in 50 mM potassium phosphate buffer, pH 6.0 was added to the wells to a final volume of 220 μL. Each plate also contained four wells treated with buffer alone that functioned as no dispersal controls (0% dispersal). The plates were incubated with enzyme for 90 min at 25 °C, and then the buffer solution was removed, and the plates were washed gently but thoroughly with deionized (DI) water to remove any nonadherent biomass. Remaining adherent cells were fixed with MeOH (200 μL) for 1 h after which the wells were aspirated and allowed to fully dry. The wells were then stained with 1% crystal violet (200 μL) for 5 min before washing thoroughly with DI water until the water ran clear. To release the bound crystal violet, 200 μL of 33% acetic acid were added to each well. A 50 μL aliquot of each sample was transferred to a new 96 well microtitre plate and diluted to 200 μL with 33% acetic acid and the absorbance of each well was measured at 590 nm using a plate reader. After subtracting the background absorbance at 590 nm for the sterile media control wells, the relative biofilm biomass remaining was calculated by dividing the absorbance at 590 nm by the average absorbance of the no dispersal control wells from each plate. The relative biofilm biomass was plotted as a function of enzyme concentration to determine IC_{50} values for biofilm dispersal. IC_{50} values were determined by fitting the data using a three-parameter inhibitor dose response curve as implemented in GRAPHPAD PRISM 9 software (GraphPad, San Diego, CA, USA) from at least three replicate experiments. The residual biofilm biomass remaining was also determined from the IC_{50} fit for each replicate experiment. Each enzyme concentration was analysed in different positions on the 96-well plate to minimize artefacts from edge effects. Statistical significance of the IC_{50} values and residual biofilm biomass relative to $DspB_{wt}$ were determined using a Welch's t-test as implemented in GRAPHPAD PRISM 9 software.

Acknowledgements

This work was funded in part by startup funds from the University of Maryland College Park and a Faculty Student Research Award from the Graduate School at University of Maryland College Park. The authors thank D. Fushman for assistance with data fitting and helpful suggestions. The authorsare grateful to F. Chen and Y. Li for assistant with analytical NMR and mass spectrometry services.

Conflict of interest

The authors declare no conflict of interest.

Author contributions

MBP, APB and SW designed all experiments. SW synthesized trisaccharides **1–3**. APB, KNM, and LLB carried out all mutagenesis, activity and biofilm dispersal assays. MBP and APB performed data analysis. APB and MBP wrote the article. All authors edited and approved the final manuscript.

Data availability statement

The data to support these results are reported in Figs 1–3, Tables 1–2 and in the supplementary information of this article. NMR spectra supporting the characterization of trisaccharides **5** and **6** are shown in supplemental Figs S1–S4. Any other data or additional information are available from the corresponding author [mpoulin@umd.edu] upon reasonable request.

References

1 Flemming H-C, Wingender J. The biofilm matrix. *Nat Rev Microbiol*. 2010;**8**:623–33.
2 Costerton JW, Stewart PS, Greenberg EP. Bacterial biofilms: a common cause of persistent infections. *Science*. 1999;**284**:1318–22.
3 Koo H, Yamada KM. Dynamic cell–matrix interactions modulate microbial biofilm and tissue 3D microenvironments. *Curr Opin Cell Biol*. 2016;**42**:102–12.
4 Nadell CD, Drescher K, Wingreen NS, Bassler BL. Extracellular matrix structure governs invasion resistance in bacterial biofilms. *ISME J*. 2015;**9**:1700–9.
5 Hobley L, Harkins C, MacPhee CE, Stanley-Wall NR. Giving structure to the biofilm matrix: an overview of individual strategies and emerging common themes. *FEMS Microbiol Rev*. 2015;**39**:649–69.
6 Vuong C, Voyich JM, Fischer ER, Braughton KR, Whitney AR, DeLeo FR, et al. Polysaccharide intercellular adhesin (PIA) protects *Staphylococcus epidermidis* against major components of the human innate immune system. *Cell Microbiol*. 2004;**6**:269–75.
7 Vuong C, Kocianova S, Voyich JM, Yao Y, Fischer ER, DeLeo FR, et al. A crucial role for exopolysaccharide modification in bacterial biofilm formation, immune evasion, and virulence. *J Biol Chem*. 2004;**279**:54881–6.
8 Yan J, Bassler BL. Surviving as a community: antibiotic tolerance and persistence in bacterial biofilms. *Cell Host Microbe*. 2019;**26**:15–21.
9 Lewis K. Riddle of biofilm resistance. *Antimicrob Agents Chemother*. 2001;**45**:999–1007.
10 Jamal M, Ahmad W, Andleeb S, Jalil F, Imran M, Nawaz MA, et al. Bacterial biofilm and associated infections. *J Chin Med Assoc*. 2018;**81**:7–11.
11 Joo H-S, Otto M. Molecular basis of in vivo biofilm formation by bacterial pathogens. *Chem Biol*. 2012;**19**:1503–13.
12 Kaplan JB. Biofilm matrix-degrading enzymes. *Methods Mol Biol*. 2014;**1147**:203–13.
13 Kaplan JB. Biofilm dispersal: mechanisms, clinical implications, and potential therapeutic uses. *J Dent Res*. 2010;**89**:205–18.
14 Nijland R, Hall MJ, Burgess JG. Dispersal of biofilms by secreted, matrix degrading, bacterial DNase. *PLoS One*. 2010;**5**:e15668.
15 Landini P, Antoniani D, Burgess JG, Nijland R. Molecular mechanisms of compounds affecting bacterial biofilm formation and dispersal. *Appl Microbiol Biotechnol*. 2010;**86**:813–23.
16 Kaplan JB, Ragunath C, Ramasubbu N, Fine DH. Detachment of *Actinobacillus actinomycetemcomitans* biofilm cells by an endogenous β-hexosaminidase activity. *J Bacteriol*. 2003;**185**:4693–8.
17 Itoh Y, Wang X, Hinnebusch BJ, Preston JF, Romeo T. Depolymerization of β-1,6-N-acetyl-D-glucosamine disrupts the integrity of diverse bacterial biofilms. *J Bacteriol*. 2005;**187**:382–7.
18 Kaplan JB, Ragunath C, Velliyagounder K, Fine DH, Ramasubbu N. Enzymatic detachment of *Staphylococcus epidermidis* biofilms. *Antimicrob Agents Chemother*. 2004;**48**:2633–6.
19 Heilmann C, Schweitzer O, Gerke C, Vanittanakom N, Mack D, Götz F. Molecular basis of intercellular adhesion in the biofilm-forming *Staphylococcus epidermidis*. *Mol Microbiol*. 1996;**20**:1083–91.
20 Mack D, Fischer W, Krokotsch A, Leopold K, Hartmann R, Egge H, et al. The intercellular adhesin involved in biofilm accumulation of *Staphylococcus epidermidis* is a linear beta-1,6-linked glucosaminoglycan: purification and structural analysis. *J Bacteriol*. 1996;**178**:175–83.
21 Cramton SE, Gerke C, Schnell NF, Nichols WW, Götz F. The intercellular adhesion (ica) locus is present in *Staphylococcus aureus* and is required for biofilm formation. *Infect Immun*. 1999;**67**:5427–33.
22 Wang X, Preston JF, Romeo T. The *pgaABCD* locus of *Escherichia coli* promotes the synthesis of a polysaccharide adhesin required for biofilm formation. *J Bacteriol*. 2004;**186**:2724–34.
23 Chen K-M, Chiang M-K, Wang M, Ho H-C, Lu M-C, Lai Y-C. The role of *pgaC* in *Klebsiella pneumoniae* virulence and biofilm formation. *Microb Pathog*. 2014;**77**:89–99.
24 Choi AHK, Slamti L, Avci FY, Pier GB, Maira-Litran T. The *pgaABCD* locus of *Acinetobacter baumannii* encodes the production of poly-β-1-6-*N*-acetylglucosamine, which is critical for biofilm formation. *J Bacteriol*. 2009;**191**:5953–63.
25 Sadovskaya I, Vinogradov E, Flahaut S, Kogan G, Jabbouri S. Extracellular carbohydrate-containing polymers of a model biofilm-producing strain, *Staphylococcus epidermidis* RP62A. *Infect Immun*. 2005;**73**:3007–17.
26 Joyce JG, Abeygunawardana C, Xu Q, Cook JC, Hepler R, Przysiecki CT, et al. Isolation, structural characterization, and immunological evaluation of a high-molecular-weight exopolysaccharide from *Staphylococcus aureus*. *Carbohydr Res*. 2003;**338**:903–22.
27 Maira-Litrán T, Kropec A, Abeygunawardana C, Joyce J, Mark G, Goldmann DA, et al. Immunochemical properties of the staphylococcal poly-*N*-acetylglucosamine surface polysaccharide. *Infect Immun*. 2002;**70**:4433–40.
28 Itoh Y, Rice JD, Goller C, Pannuri A, Taylor J, Meisner J, et al. Roles of *pgaABCD* genes in synthesis, modification, and export of the *Escherichia coli* biofilm adhesin poly-β-1,6-*N*-acetyl-D-glucosamine. *J Bacteriol*. 2008;**190**:3670–80.

29 Kaplan JB, Mlynek KD, Hettiarachchi H, Alamneh YA, Biggemann L, Zurawski DV, et al. Extracellular polymeric substance (EPS)-degrading enzymes reduce staphylococcal surface attachment and biocide resistance on pig skin in vivo. *PLoS One*. 2018;**13**: e0205526–13.
30 Little DJ, Pfoh R, Mauff FL, Bamford NC, Notte C, Baker P, et al. PgaB orthologues contain a glycoside hydrolase domain that cleaves deacetylated poly-β-(1,6)-*N*-acetylglucosamine and can disrupt bacterial biofilms. *PLoS Pathog*. 2018;**14**:e1006998-29.
31 Wang S, Breslawec AP, Alvarez E, Tyrlik M, Li C, Poulin MB. Differential recognition of deacetylated PNAG oligosaccharides by a biofilm degrading glycosidase. *ACS Chem Biol*. 2019;**9**:1998–2005.
32 Breslawec AP, Wang S, Li C, Poulin MB. Anionic amino acids support hydrolysis of poly-β-(1,6)-*N*-acetylglucosamine exopolysaccharides by the biofilm dispersing glycosidase Dispersin B. *J Biol Chem*. 2021;**296**:100203.
33 Fazekas E, Kandra L, Gyémánt G. Model for β-1,6-N-acetylglucosamine oligomer hydrolysis catalyzed by DispersinB, a biofilm degrading enzyme. *Carbohydr Res*. 2012;**363**:7–13.
34 Manuel SGA, Ragunath C, Sait HBR, Izano EA, Kaplan JB, Ramasubbu N. Role of active-site residues of dispersin B, a biofilm-releasing β-hexosaminidase from a periodontal pathogen, in substrate hydrolysis. *FEBS J*. 2007;**274**:5987–99.
35 Williams SJ, Mark BL, Vocadlo DJ, James MNG, Withers SG. Aspartate 313 in the *Streptomyces plicatus* hexosaminidase plays a critical role in substrate-assisted catalysis by orienting the 2-acetamido group and stabilizing the transition state. *J Biol Chem*. 2002;**277**:40055–65.
36 Tews I, Perrakis A, Oppenheim A, Dauter Z, Wilson KS, Vorgias CE. Bacterial chitobiase structure provides insight into catalytic mechanism and the basis of Tay–Sachs disease. *Nat Struct Biol*. 1996;**3**:638–48.
37 Montgomery EM, Richtmyer NK, Hudson CS. Attempts to find new antimalarials. VIII. 1-Phenyl-β-D-glucothiosides, diphenyl disulfides, phenyl thiocyatates, and related compounds. *J Org Chem*. 1946;**11**:301–6.

Supporting information

Additional supporting information may be found online in the Supporting Information section at the end of the article.

Fig. S1. ^{1}H NMR spectra for compound 6.
Fig. S2. ^{13}C NMR spectra for compound 6.
Fig. S3. ^{1}H NMR spectra for compound 3.
Fig. S4. ^{13}C NMR spectra for compound 3.